



A Lagrange multiplier method for a discrete fracture model for flow in porous media

Markus Köppel¹ · Vincent Martin² · Jérôme Jaffré³ · Jean E. Roberts³

Received: 31 January 2018 / Accepted: 11 September 2018 / Published online: 25 September 2018
© Springer Nature Switzerland AG 2018

Abstract

In this work, we present a novel discrete fracture model for single-phase Darcy flow in porous media with fractures of co-dimension one, which introduces an additional unknown at the fracture interface. Inspired by the fictitious domain method, this Lagrange multiplier couples fracture and matrix domain and represents a local exchange of the fluid. The multipliers naturally impose the equality of the pressures at the fracture interface. The model is thus appropriate for domains with fractures of permeability higher than that in the surrounding bulk domain. In particular, the novel approach allows for independent, regular meshing of fracture and matrix domain and therefore avoids the generation of small elements. We show existence and uniqueness of the weak solution of the continuous primal formulation. Moreover, we discuss the discrete inf-sup condition of two different finite element formulations. Several numerical examples verify the accuracy and convergence of proposed method.

Keywords Discrete fracture model · Porous media · Finite element method · Lagrange multiplier method · Nonconforming grids

1 Introduction

The subsurface of the earth generally contains a variety of heterogeneous features such as different geological formations, inclusions, and fractures. The material parameters in the domain of interest thus may vary by several orders of magnitude. This often leads to a significant change

in the flow behavior, in particular if large fractures are present. A fracture is characterized by its lateral dimension which is considerably smaller than its extension in other directions. Depending on their hydrogeological properties, fractures may act as barriers and/or conduits to the flow. Common examples of domains of application in the Earth sciences include CO₂ sequestration below caprock formations, underground storage of radioactive waste, geothermal energy production, and enhanced oil recovery. In the last few decades, the inclusion of fractures in models for flow in porous media has received more and more attention, and a variety of different models have been proposed.

In principle, fractured porous media models can be categorized roughly as either discrete fracture-matrix (DFM) models or continuum fracture models. Since the proposed method requires information concerning the location of the fractures in the domain of interest and since the method calculates the flow in the fracture as well as in the surrounding domain, we will focus mainly on DFM models in the remainder of this article. We refer to, e.g., [11, 51] for a more general overview of flow models for fractured porous media. Because of their aforementioned geometries, a common way to incorporate fractures in a DFM model is to consider them as $(n - 1)$ -dimensional

✉ Markus Köppel
markus.koeppel@ians.uni-stuttgart.de

Vincent Martin
vincent.martin@utc.fr

Jérôme Jaffré
jerome.jaffre@inria.fr

Jean E. Roberts
jean-elizabeth.roberts@inria.fr

¹ IANS, Universität Stuttgart, Pfaffenwaldring 57, 70569 Stuttgart, Germany

² LMAC, Université de Technologie de Compiègne (UTC), Rue du docteur Schweitzer CS 60310, 60203 Compiègne Cedex, France

³ INRIA Paris, 2 Rue Simone IFF, 75012 Paris, France

objects within the surrounding n -dimensional matrix (bulk) domain. This approach avoids the generation of small elements of the spatial discretization grid in (the vicinity of) the fracture and reduces the computational costs. Additionally, it is often assumed that the fracture is filled with debris which facilitates the modeling by making it appropriate to use Darcy's law in both the fracture and matrix parts of the domain. Such models have been extensively studied from the mathematical and/or the engineering point of view. Many of these studies are concerned with linear Darcy flow; see [5–7, 10, 16, 22, 26, 27, 47, 59] to name just a few. Others represent extensions to allow for Forchheimer flow in the fractures [30, 42] or for Darcy–Brinkman flow [45], and others for two-phase or multiphase flow [1, 17, 18, 31, 34, 36, 37, 39, 40, 46, 48–50], where again we cite just a few. Some articles have also taken up the topic of discrete fracture network (DFN) models, e.g., [12, 13, 52]. Various numerical discretization methods have been used: finite element methods [10, 41], mixed or mixed-hybrid finite elements [5, 6, 47], finite volume methods [7, 26, 36, 40, 53, 55], multi-point flux methods [2, 3, 55], mimetic finite difference methods [9], discontinuous Galerkin methods [8], and vertex approximate -gradient methods [16, 17]. Still, another approach was given in [15].

In many articles, the fracture elements, of co-dimension one with respect to the matrix domain, coincide with the faces of the matrix elements. This configuration is generally referred to as a matching fracture and matrix grid approach. However, one may wish to discretize the fracture more finely in the case of a highly conductive fracture or more coarsely in the case of a barrier and methods allowing for non-matching grids may be used; see, e.g., [27, 29, 59]. Still with these methods, the fracture cannot cut through the interior of a matrix element; it must lie in the union of the faces of the matrix elements. The matrix grid must be aligned with the fracture.

Nonconforming methods, on the other hand, are characterized by an independent meshing of the fracture and the matrix domain which allows for regular meshes and elements in the corresponding domains. The most prominent example in the field of nonconforming methods is the extended finite element method (XFEM), e.g., in [22, 38, 56] for the primal formulation and in [23, 32] for the dual formulation, where the respective basis functions are locally enriched in the vicinity of the fracture to account for the discontinuities.

This paper presents an alternative nonconforming formulation. The method uses Lagrange multiplier variables in a primal variational formulation to connect the fracture flow with the flow in the matrix. The multipliers approximate the jump of the normal flux across the fracture interface and represent the exchange between the fracture and the matrix.

Using the ideas of [35], we show that the continuous problem is well posed. In this paper, the pressure is assumed to be continuous across the fracture, i.e., the permeability in the fracture is assumed to be larger than in the matrix. The case of geological barriers is thus excluded from the current study. The discretization uses Lagrange \mathbb{P}^1 finite elements both in the matrix and in the fracture, and since the exchanges between the fracture and matrix flow are only through Lagrange multipliers, the grids for the matrix and the fracture can be mutually independent. The multipliers are discretized by either piecewise constant or continuous, piecewise linear basis functions on the fracture interface provided that the involved mesh size is not too small compared to the matrix mesh. We show the inf-sup stability of the first of these, again following ideas of [35]. Somewhat surprisingly, the fracture flow equation does not figure in the proof of the stability and the pressure fracture mesh can be chosen arbitrarily. In a companion paper [44], we study a different discretization with a consistent penalty term to stabilize the system and a different way of treating the mesh compatibility issue.

The remainder of the paper is organized as follows: in Section 2, we give the continuous formulation of the Lagrange multiplier, finite element method and prove the existence and uniqueness of the weak solution for a domain of dimension 2 or 3. Section 3 concerns the discrete formulations of the problem and the proof of their well-posedness. For this part, we have considered only the case of a 2 dimensional domain. In Section 4, we analyze the method by means of several numerical examples of different complexity. We perform a numerical error and convergence analysis to study the constraints on the mesh size of the multipliers and the performance of the method in more detail. Finally, we conclude and discuss the proposed method in Section 5.

2 A Lagrange multiplier formulation of the continuous problem

We consider a convex, matrix domain $\Omega \subset \mathbb{R}^n$, $n = 2$ or 3 , and a fracture domain $\gamma \subset \Omega$ of dimension $n - 1$, with a continuous unit vector field \mathbf{n}_γ normal to the fracture-surface γ , see Fig. 1. For simplicity, we assume that the

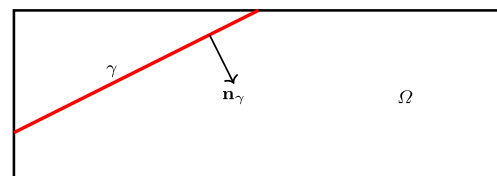


Fig. 1 Example of a domain containing a fracture

fracture γ is a line segment if $n = 2$ and a planar surface if $n = 3$, and that $\partial\gamma \subset \partial\Omega$. Also for simplicity, homogeneous Dirichlet boundary conditions on $\partial\Omega$ and on $\partial\gamma$ are imposed.

Flow in Ω is governed by

$$\begin{aligned} \operatorname{div}(-\mathbf{K}\nabla p) &= f && \text{in } \Omega \\ p &= 0 && \text{on } \Gamma = \partial\Omega \end{aligned} \tag{1}$$

and in γ by

$$\begin{aligned} \operatorname{div}_\gamma(-\mathbf{K}_\gamma \nabla_\gamma p_\gamma) &= f_\gamma && \text{in } \gamma \\ p_\gamma &= 0 && \text{on } \partial\gamma, \end{aligned} \tag{2}$$

where $\operatorname{div}_\gamma$ and ∇_γ are the $(n - 1)$ -dimensional divergence and gradient operators in the plane of γ , the coefficients \mathbf{K} and \mathbf{K}_γ are the symmetric, uniformly positive-definite, bounded, permeability tensor-fields on Ω and γ respectively, the unknowns p and p_γ represent the fluid pressure, and f and f_γ external source terms. However, to permit the possibility of fluid exchange between Ω and γ , we introduce a term $\lambda = \lambda(x)$, $x \in \gamma$ that will be added in as a source/sink term in γ and subtracted out as a sink/source term in Ω at its intersection with γ . Thus, Eqs. 1 and 2 become

$$\begin{aligned} \operatorname{div}(-\mathbf{K}\nabla p) - \lambda &= f, && \text{in } \Omega, \\ p &= 0, && \text{on } \Gamma = \partial\Omega, \end{aligned} \tag{3}$$

and

$$\begin{aligned} \operatorname{div}_\gamma(-\mathbf{K}_\gamma \nabla_\gamma p_\gamma) + \lambda &= f_\gamma, && \text{in } \gamma, \\ p_\gamma &= 0, && \text{on } \partial\gamma. \end{aligned} \tag{4}$$

To obtain a variational formulation, we will multiply by test functions q and q_γ , integrate over Ω and γ , and use integration by parts in both equations. Define the spaces V_Ω , V_γ , \mathbf{V} , and Λ as follows:

$$\begin{aligned} V_\Omega &= H_0^1(\Omega), && V_\gamma = H_0^1(\gamma), \\ \mathbf{V} &= V_\Omega \times V_\gamma, && \Lambda = H_{0,0}^{-\frac{1}{2}}(\gamma). \end{aligned} \tag{5}$$

These spaces are endowed with the following norms: for $q \in V_\Omega$, for $q_\gamma \in V_\gamma$, and for $\mu \in \Lambda$,

$$\begin{aligned} \|q\|_{V_\Omega}^2 &= \|q\|_{0,\Omega}^2 + \|\nabla q\|_{0,\Omega}^2, \\ \|q_\gamma\|_{V_\gamma}^2 &= \|q_\gamma\|_{0,\gamma}^2 + \|\nabla_\gamma q_\gamma\|_{0,\gamma}^2, \\ \|(q, q_\gamma)\|_{\mathbf{V}}^2 &= \|q\|_{V_\Omega}^2 + \|q_\gamma\|_{V_\gamma}^2, \\ \|\mu\|_\Lambda &= \sup_{\xi \in H_{0,0}^{\frac{1}{2}}(\gamma)} \frac{\int_\gamma \mu, \xi}{\|\xi\|_{H_{0,0}^{\frac{1}{2}}(\gamma)}}, \end{aligned} \tag{6}$$

where $\|\cdot\|_{0,\mathcal{O}}$ denotes the standard $L^2(\mathcal{O})$ norm on an open set \mathcal{O} , where $\|\cdot\|_{H_{0,0}^{\frac{1}{2}}(\gamma)}$ is defined by $\|\xi\|_{H_{0,0}^{\frac{1}{2}}(\gamma)} = \inf_{q \in V_\Omega} \|q\|_{V_\Omega}$, where for $q \in V_\Omega$, $q|_\gamma$ denotes the trace $q|_\gamma = \xi$

of q on γ , and where $\int_\gamma \mu \xi$ denotes the duality pairing $\langle \cdot, \cdot \rangle_\gamma$ between $H_{0,0}^{-\frac{1}{2}}(\gamma)$ and $H_{0,0}^{\frac{1}{2}}(\gamma)$. The variational formulation is then given as follows:

Find $(p, p_\gamma) \in \mathbf{V}$ and $\lambda \in \Lambda$ such that

$$\begin{aligned} \int_\Omega \mathbf{K}\nabla p \cdot \nabla q + \int_\gamma \mathbf{K}_\gamma \nabla_\gamma p_\gamma \cdot \nabla_\gamma q_\gamma \\ - \int_\gamma \lambda(q|_\gamma - q_\gamma) &= \int_\Omega f q + \int_\gamma f_\gamma q_\gamma && \forall (q, q_\gamma) \in \mathbf{V} \\ \int_\gamma (p|_\gamma - p_\gamma)\mu &= 0 && \forall \mu \in \Lambda, \end{aligned} \tag{7}$$

where the Lagrange multiplier can be interpreted as the jump across the fracture of the normal component of the product of the permeability tensor with the gradient of the matrix pressure, i.e., $\lambda = \llbracket \mathbf{K}\nabla p \cdot \mathbf{n}_\gamma \rrbracket_\gamma$.

Problem (7) is a Lagrange multiplier primal formulation that corresponds to the fracture problem that was studied in [5, 6] in mixed form. Then, defining the bilinear forms $a : \mathbf{V} \times \mathbf{V} \rightarrow \mathbb{R}$ and $b : \mathbf{V} \times \Lambda \rightarrow \mathbb{R}$ and the linear form $\ell : \mathbf{V} \rightarrow \mathbb{R}$ by

$$\begin{aligned} a((p, p_\gamma), (q, q_\gamma)) &= \int_\Omega \mathbf{K}\nabla p \cdot \nabla q + \int_\gamma \mathbf{K}_\gamma \nabla_\gamma p_\gamma \cdot \nabla_\gamma q_\gamma, \\ b(p, p_\gamma; \mu) &= \int_\gamma (p|_\gamma - p_\gamma)\mu, \\ \ell(q, q_\gamma) &= \int_\Omega f q + \int_\gamma f_\gamma q_\gamma, \end{aligned} \tag{8}$$

we may write (7) in standard mixed form,

Find $(p, p_\gamma) \in \mathbf{V}$ and $\lambda \in \Lambda$ such that

$$\begin{aligned} a((p, p_\gamma), (q, q_\gamma)) - b(q, q_\gamma; \lambda) &= \ell(q, q_\gamma), && \forall (q, q_\gamma) \in \mathbf{V} \\ b(p, p_\gamma; \mu) &= 0, && \forall \mu \in \Lambda, \end{aligned} \tag{9}$$

and, following the techniques of [35], prove the following theorem:

Theorem 1 *There exists a unique solution to the continuous Lagrange multiplier, fracture problem (9).*

Proof It is easily seen that the bilinear forms a and b are continuous and that, in light of the hypotheses made concerning \mathbf{K} and \mathbf{K}_γ , a is elliptic on all of \mathbf{V} . Thus, in order to show the existence and uniqueness of the solution of Eq. 9 using the classical results of Brezzi [14, 20, 54], we have only to show that $b(\cdot, \cdot)$ satisfies an inf-sup condition,

more precisely, to show that there exists a positive constant θ_b such that

$$\inf_{\mu \in \Lambda} \sup_{(q, q_\gamma) \in \mathbf{V}} \frac{b(q, q_\gamma; \mu)}{\|\mu\|_\Lambda \|(q, q_\gamma)\|_{\mathbf{V}}} \geq \theta_b.$$

Toward this end, recalling the definitions of the Λ norm (6) and of the $H_{0,0}^{\frac{1}{2}}(\gamma)$ norm, we note that for each $\mu \in \Lambda$

$$\begin{aligned} \sup_{(q, q_\gamma) \in \mathbf{V}} \frac{b(q, q_\gamma; \mu)}{\|\mu\|_\Lambda \|(q, q_\gamma)\|_{\mathbf{V}}} &\geq \sup_{(q, 0) \in \mathbf{V}} \frac{b(q, 0; \mu)}{\|\mu\|_\Lambda \|(q, 0)\|_{\mathbf{V}}} \\ &= \sup_{q \in V_\Omega} \frac{\langle \mu, q|_\gamma \rangle_\gamma}{\|\mu\|_\Lambda \|q\|_{V_\Omega}} \\ &= \sup_{\xi \in H_{0,0}^{\frac{1}{2}}(\gamma)} \sup_{\substack{q \in V_\Omega \\ q|_\gamma = \xi}} \frac{\langle \mu, \xi \rangle_\gamma}{\|\mu\|_\Lambda \|q\|_{V_\Omega}} \\ &= \sup_{\xi \in H_{0,0}^{\frac{1}{2}}(\gamma)} \left(\frac{\langle \mu, \xi \rangle_\gamma}{\|\mu\|_\Lambda} \frac{1}{\inf_{\substack{q \in V_\Omega \\ q|_\gamma = \xi}} \|q\|_{V_\Omega}} \right) \\ &= \sup_{\xi \in H_{0,0}^{\frac{1}{2}}(\gamma)} \frac{\langle \mu, \xi \rangle_\gamma}{\|\mu\|_\Lambda \|\xi\|_{H_{0,0}^{\frac{1}{2}}(\gamma)}} = 1. \end{aligned}$$

□

3 Discretization

In this section, we are concerned with formulating and analyzing a discrete counterpart to Eq. 9. The discrete formulation is based on three distinct meshes, one for the approximation of the pressure in the domain Ω , one for the approximation of the pressure in the fracture γ , and one for the approximation of the Lagrange multiplier in the fracture. We will in fact consider two discrete problems which will differ in the choice of the space of Lagrange multipliers. In one the multipliers are piecewise constant and in the other they are continuous, piecewise linear functions on γ . For the case of piecewise constant multipliers, existence and uniqueness as well as convergence are proved, following the ideas of [35], under the hypothesis that the Lagrange multiplier space is not too rich with respect to the space for the approximation of the matrix pressure, i.e., when the Lagrange multiplier mesh size h_λ is not too small with respect to the matrix pressure mesh size h ; see Hypothesis 1 and Remark 1. The numerical experiments of Section 4 give accurate results when $h_\lambda \geq 2h$. For the case of continuous multipliers, existence and uniqueness are shown for the case that the mesh, and indeed the approximation space, for the Lagrange multipliers is the same as that for the fracture pressure. We were not able to show convergence in this case; however, the numerical results are more than encouraging, see Section 4.

For the remainder of this article, we restrict our attention to the two-dimensional setting, i.e., we suppose that Ω is two-dimensional and γ is one-dimensional. We see no inherent reason why the same procedure could not be used in a three-dimensional setting though it would of course be more technically complex and much more involved to implement numerically.

3.1 Approximation spaces and a discrete formulation

To discretize problem (9), we let \mathcal{T}_h be a finite element discretization of Ω made up of triangles and/or rectangles, and let both $\mathcal{T}_{h,\gamma}$ and $\mathcal{T}_{h,\lambda}$ be discretizations of γ (made up of line segments), and we let h, h_γ , and h_λ denote the respective mesh sizes:

$$\begin{aligned} h &= \max_{T \in \mathcal{T}_h} h_T \text{ where } h_T = \text{diam } T, \\ h_\gamma &= \max_{t \in \mathcal{T}_{h,\gamma}} h_t \text{ where } h_t = \text{diam } t, \\ h_\lambda &= \max_{s \in \mathcal{T}_{h,\lambda}} h_s \text{ where } h_s = \text{diam } s. \end{aligned}$$

We assume that each of these grids belongs to a family of discretizations that is regular, and \mathcal{T}_h to a family that is uniformly regular in the sense that there is a positive constant σ_Ω such that for each h ,

$$\frac{h}{\rho_h} \leq \sigma_\Omega, \text{ with } \rho_h = \min_{T \in \mathcal{T}_h} \rho_T \text{ and } \rho_T = \text{inradius } T.$$

We will also make use of the notation $\sigma_T = h_T / \rho_T$.

Let $V_{h,\Omega}$ and $V_{h,\gamma}$ respectively be the space of continuous, piecewise-bilinear (piecewise-affine) functions on Ω and on γ respectively which vanish on $\partial\Omega$ and on $\partial\gamma$ respectively:

$$V_{h,\Omega} = \left\{ q \in H_0^1(\Omega) : \forall T \in \mathcal{T}_h, \right. \\ \left. q|_T \in \begin{cases} \mathbb{P}^1(T) & \text{if } T \text{ is a triangle} \\ \mathbb{Q}^{1,1}(T) & \text{if } T \text{ is a rectangle} \end{cases} \right\}, \tag{10}$$

$$V_{h,\gamma} = \{q_\gamma \in H_0^1(\gamma) : \forall t \in \mathcal{T}_{h,\gamma}, q_\gamma|_t \in \mathbb{P}^1(t)\}.$$

Then \mathbf{V}_h will denote $V_{h,\Omega} \times V_{h,\gamma}$:

$$\mathbf{V}_h = V_{h,\Omega} \times V_{h,\gamma}.$$

For the approximation of the Lagrange multiplier λ , we will consider two different discrete spaces Λ_h which are defined in Sections 3.2 and 3.3, respectively. Each of these choices for Λ_h gives rise to a discrete problem whose variational formulation may be expressed as follows:

$$\begin{aligned} \text{Find } (p_h, p_{\gamma,h}) \in \mathbf{V}_h \text{ and } \lambda_h \in \Lambda_h \text{ such that} \\ a((p_h, p_{\gamma,h}), (q_h, q_{\gamma,h})) - b(q_h, q_{\gamma,h}; \lambda_h) &= \ell(q_h, q_{\gamma,h}), \\ &\forall (q_h, q_{\gamma,h}) \in \mathbf{V}_h \\ b(p_h, p_{\gamma,h}; \mu_h) &= 0, \\ &\forall \mu_h \in \Lambda_h. \end{aligned} \tag{11}$$

Clearly, on the discrete approximation spaces V_h , the bilinear form a is both continuous and elliptic and both of these uniformly in h .

3.2 A piecewise constant Lagrange multiplier space

For the approximation of the Lagrange multiplier λ , we define the approximation space Λ_h as follows:

$$\Lambda_h = \{\lambda_h \in L^2(\gamma) \mid \lambda_h|_s \in \mathbb{P}^0(s), \forall s \in \mathcal{T}_{h,\lambda}\}. \tag{12}$$

With this definition, the bilinear form b is continuous on $V_h \times \Lambda_h$ with a constant of continuity that is independent of h . Thus, to apply the standard Brezzi theory for mixed formulations and obtain existence and uniqueness of the solution of the discrete problem and to obtain error estimates, we need only establish a uniform-in- h , discrete inf-sup condition. As in the proof of Theorem 1, we actually show the inf-sup condition for b on $(V_\Omega \times 0) \times \Lambda$, we need only define for each h , a continuous projection operator $\Pi_h : V_\Omega \rightarrow V_{h,\Omega}$ in such a way that the family of projections operators is stable in the sense that the constant of continuity is independent of h , and such that $\forall h$ the following diagram commutes:

$$\begin{array}{ccc} V_\Omega & \xrightarrow{\tau} & H_{0,0}^{\frac{1}{2}}(\gamma) \\ \downarrow \Pi_h & & \downarrow \pi_{L^2} \\ V_{h,\Omega} & \xrightarrow{\pi_{L^2} \circ \tau} & \Lambda_h \end{array}$$

where $\tau : V_\Omega \rightarrow H_{0,0}^{\frac{1}{2}}(\gamma)$ denotes the trace map and $\pi_{L^2} : L^2(\gamma) \rightarrow \Lambda_h$ the L^2 -projection operator onto Λ_h .

Following [35], we will define the continuous operators Π_h such that there exists a constant C_Π independent of h such that the following two conditions are satisfied:

Condition 1 $\forall p \in V_\Omega, \quad \|\Pi_h p\|_{1,\Omega} \leq C_\Pi \|p\|_{1,\Omega},$

Condition 2 $\forall p \in V_\Omega, \text{ and } \forall \mu_h \in \Lambda_h,$
 $b(p - \Pi_h p, 0; \mu_h) = 0.$

To define such an operator Π_h , we will use the Scott-Zhang projection [57], but in order to have Condition 2, we will need to modify this projection operator in the vicinity of γ , and for this we will need a compatibility condition between \mathcal{T}_h and $\mathcal{T}_{h,\lambda}$. The mesh $\mathcal{T}_{h,\gamma}$ does not come into play. We first define some notation associated with the mesh \mathcal{T}_h . For $T \in \mathcal{T}_h$, let Δ_T denote the interior of the union of the closures of the elements $T' \in \mathcal{T}_h$ sharing a boundary point with T , and for a vertex a of some $T \in \mathcal{T}_h$, let Δ_a denote the interior of the union of the closures of the elements $T' \in \mathcal{T}_h$ having a as a vertex, see Fig. 2. For y and z in Ω , let \overline{yz}

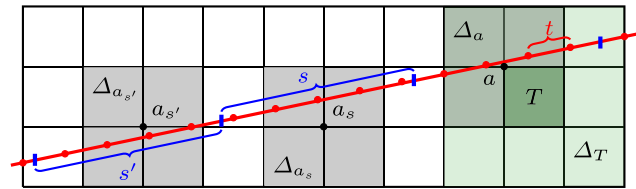


Fig. 2 Construction and support of macro elements. Here, all of the elements T are rectangles, but the case of triangular elements is similar. Patches of elements Δ_T are in shades of green and patches of vertices Δ_a are depicted in grey

denote the line segment between y and z and $|yz|$ its length. The condition of compatibility between the meshes \mathcal{T}_h and $\mathcal{T}_{h,\lambda}$ needed to define the operators Π_h is that the following hypothesis holds:

Hypothesis 1 *To each $s \in \mathcal{T}_{h,\lambda}$, a vertex a_s (of a cell in \mathcal{T}_h) may be associated in such a way that*

- *there is an edge e_s of a cell of \mathcal{T}_h and a point $x_s \in (e_s \cap s)$ such that a_s is an endpoint of e_s and $|a_s x_s| \leq |x_s b_s|$ where b_s is the other endpoint of e_s ,*
- *neither endpoint of s belongs to Δ_{a_s}*
- *if s and s' are distinct elements of $\mathcal{T}_{h,\lambda}$, then $\Delta_{a_s} \cap \Delta_{a_{s'}} = \emptyset$.*

Note that Hypothesis 1 does not exclude the case in which the fracture γ passes through a vertex. (It is possible in some cases to choose for a_s a vertex lying on s and to take $x_s = a_s$). Neither does it exclude the case in which γ lies along one or more of the edges of the cells of \mathcal{T}_h . (One can choose the edge e_s to be a subset of s .)

Remark 1 Hypothesis 1 is satisfied if $3h < |s|, \forall s \in \mathcal{T}_{h,\lambda}$, cf. [35].

For the demonstrations, we will also need a second hypothesis:

Hypothesis 2 *There exists an L such that $|s| \leq Lh, \forall s \in \mathcal{T}_{h,\lambda}$.*

Remark 2 As the fracture is supposed to be at least as permeable as the matrix domain, normally one would take $h_\gamma \leq h$; however, neither the ratio h/h_γ nor h_λ/h_γ is used in the proofs.

Remark 3 The two Conditions, 1 and 2, are necessary and sufficient to prove the stability of problem (11). Hypotheses 1 and 2 taken together are sufficient to obtain these two Conditions, see Lemma 3, but are not necessary in general. In particular, the practical requirement on the meshes $3h < |s|$ (see Remark 1) can often be relaxed, see Section 4.

3.2.1 A multiplicative trace lemma

Before establishing approximation, results we give a multiplicative trace inequality.

Lemma 1 *There is a constant $C_\tau > 0$ such that if T is a triangle, ζ is a straight line segment contained in T and $q \in H^1(T)$, then*

$$\|q|_\zeta\|_{0,\zeta}^2 \leq C_\tau \sigma_T (h_T^{-1} \|q\|_{0,T}^2 + h_T \|\nabla q\|_{0,T}^2). \tag{13}$$

Proof Let T be a triangle and ζ a line segment with $\zeta \subset T$. We use a bijective affine transformation from a reference element \widehat{T} onto T . Let $\widehat{\zeta}$ denote the pre-image of ζ under this transformation, and for $q \in H^1(T)$ let $\widehat{q} \in H^1(\widehat{T})$ denote the induced function on \widehat{T} . Applying now [35, Lemma 2], which states that there is a constant \widehat{C} such that $\forall \widehat{r} \in H^1(\widehat{T})$ and for each line segment $\widehat{\xi} \subset \widehat{T}$

$$\|\widehat{r}|_{\widehat{\xi}}\|_{0,\widehat{\xi}} \leq \widehat{C} \|\widehat{r}\|_{1,\widehat{T}},$$

we obtain

$$\begin{aligned} \|q|_\zeta\|_{0,\zeta}^2 &\leq \|B_T\| \|\widehat{q}|_{\widehat{\zeta}}\|_{0,\widehat{\zeta}}^2 \\ &\leq \widehat{C}^2 \|B_T\| \|\widehat{q}\|_{1,\widehat{T}}^2 = \widehat{C}^2 \|B_T\| \left(\|\widehat{q}\|_{0,\widehat{T}}^2 + |\widehat{q}|_{1,\widehat{T}}^2 \right) \\ &\leq \widehat{C}^2 \|B_T\| |\det(B_T)|^{-1} \left(\|q\|_{0,T}^2 + \|B_T\|^2 |q|_{1,T}^2 \right) \\ &\leq c \widehat{C}^2 h_T (h_T \rho_T)^{-1} \left(\|q\|_{0,T}^2 + h_T^2 |q|_{1,T}^2 \right), \end{aligned}$$

where B_T is the linear part of the affine transformation from \widehat{T} to T , and c is independent of h_T . \square

Remark 4 Lemma 1 also holds if T is instead a rectangle. The proof is completely analogous to the one above.

This lemma cannot be derived directly from [19, Theorem 1.6.6] (together with Young’s inequality), because the constant in that Theorem depends on the domain (T here). It could though be derived from [4], using the fact that a triangle can be chosen inside T as such: it has an edge that is ζ and the minimum and maximum lengths between ζ and the opposite vertex are bounded by h_T from below and from above. Thus, one can apply [4, Lemma 10] using ζ as the edge of this particular triangle and recover an estimate similar to Eq. 13. See also [25, Lemma 9.14] for the case of L^p .

3.2.2 Existence, uniqueness, and convergence

To prove the well-posedness of Problem (11), with Λ_h defined in Eq. 12, under Hypotheses 1 and 2, following [35], we define the projection operator to be a locally corrected Scott-Zhang interpolation operator:

$$\Pi_h p = SZ_h p + \sum_{s \in \mathcal{T}_{h,\lambda}} C_s \phi_s, \quad \text{for } p \in V_\Omega, \tag{14}$$

where $SZ_h : V_\Omega \rightarrow V_{h,\Omega}$ is the Scott-Zhang interpolation operator, $\phi_s \in V_{h,\Omega}$ is the function having nodal values equal to zero except at a_s where the nodal value is 1, and the constant C_s is defined by

$$C_s = \frac{-1}{\int_s \phi_s|_s} \int_s (SZ_h p - p)|_s. \tag{15}$$

The next two lemmas show that the operator Π_h satisfies Conditions 1 and 2.

Lemma 2 *Assume that the pair of meshes $(\mathcal{T}_h, \mathcal{T}_{h,\lambda})$ satisfies Hypothesis 1. Then, there exists a constant $C_\phi > 0$ independent of h such that for each $s \in \mathcal{T}_{h,\lambda}$*

$$\int_s \phi_s|_s \geq C_\phi h.$$

Proof We give the proof for the case in which the mesh \mathcal{T}_h is a mesh of triangles. The case of rectangles is similar. For $s \in \mathcal{T}_{h,\lambda}$, let a_s, e_s, x_s , and b_s be as in Hypothesis 1. Then, e_s borders two cells lying in Δ_{a_s} . Choose one and label it T_s , and label its remaining vertex c_s , see Fig. 3, left. The angle of T_s at b_s will be denoted by \widehat{b}_s . Denote by y_s the endpoint of $T_s \cap s$ opposite x_s and by δ_s the length of $\overline{x_s y_s}$, the segment between x_s and y_s . Since ϕ_s is linear in T_s , from the definition of x_s , we have

$$\int_{T_s \cap s} \phi_s|_{T_s \cap s} = \frac{1}{2} (\phi_s(x_s) + \phi_s(y_s)) \delta_s \geq \frac{1}{4} \delta_s.$$

There remains to find a lower bound for δ_s in terms of h . There are three possible cases: in the first case $s \cap e_s = e_s$. In this case, one can take $x_s = a_s$ and $y_s = b_s$, and obviously $\delta_s = |e_s| \geq \rho_{T_s}$.

In the second case, the endpoint y_s belongs to $\overline{b_s c_s}$. Letting ℓ_{T_s} denote the perimeter of T_s , because $\sin(\widehat{b}_s) = \frac{|T_s|}{\frac{1}{2}|a_s b_s| |b_s c_s|} = \frac{\frac{1}{2} \ell_{T_s} \rho_{T_s}}{\frac{1}{2} |a_s b_s| |b_s c_s|} \geq \frac{2 h_{T_s} \rho_{T_s}}{h_{T_s}^2} = \frac{2}{\sigma_{T_s}}$, we have $\delta_s \geq |x_s b_s| \sin(\widehat{b}_s) \geq \frac{1}{2} |e_s| \sin(\widehat{b}_s) \geq \frac{1}{\sigma_{T_s}} \rho_{T_s} \geq \frac{1}{\alpha_\Omega} \rho_{T_s}$.

In the third and last case, y_s belongs to $\overline{a_s c_s}$. Here, there are two possibilities: if y_s is closer to c_s than to a_s , then $\delta_s \geq \frac{1}{2} |b_s c_s| \geq \frac{1}{2} \rho_{T_s}$. If on the other hand, y_s is closer to a_s , then redefine x_s to be y_s , e_s to be $\overline{a_s c_s}$ and T_s to be the other cell of \mathcal{T}_h having $\overline{a_s c_s}$ as an edge. Repeat the previous arguments. One may change successively the point

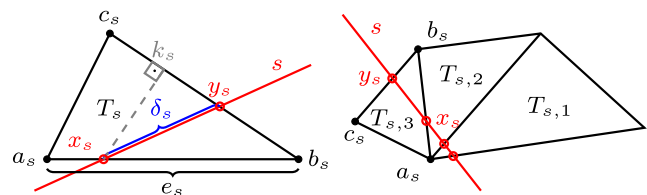


Fig. 3 Intersections of a macro element on a triangular grid

x_s , turning around a_s until reaching one of the previous cases (recall that s is a straight segment), see Fig. 3, right.

Conclude by noting that $\rho_{T_s} \geq \rho_h \geq \frac{h}{\sigma_\Omega}$, where we have used the uniform regularity of \mathcal{T}_h . \square

Lemma 3 *With Π_h defined by Eqs. 14 and 15, if the pair $(\mathcal{T}_h, \mathcal{T}_{h,\lambda})$ satisfies Hypotheses 1 and 2, then Conditions 1 and 2 are satisfied.*

Proof With the definition of C_s given in Eq. 15, it is clear that Condition 2 is satisfied. Thus, we have left to find an upper bound C_Π on the continuity constants C_{Π_h} of the operators Π_h . Since the support of ϕ_s is Δ_{a_s} , we have, for each $p \in V_\Omega$, that

$$\|\Pi_h p\|_{1,\Omega} \leq \|\mathcal{SZ}_h p\|_{1,\Omega} + \left(\sum_{s \in \mathcal{T}_{h,\lambda}} |C_s|^2 \|\phi_s\|_{1,\Delta_{a_s}}^2 \right)^{\frac{1}{2}}. \tag{16}$$

Estimates for the Scott-Zhang operator are well known, cf. [57] or [24, Lemma 1.130]:

$$\begin{aligned} \forall \ell, m, h, q; \ell > \frac{1}{2}; 0 \leq m \leq \min\{1, \ell\}, q \in H^\ell(\Omega), \\ \|\mathcal{SZ}_h q\|_{m,\Omega} &\leq C_{\mathcal{SZ}} \|q\|_{\ell,\Omega}, \\ \forall \ell, m, h, T, q; \frac{1}{2} < \ell \leq 2; 0 \leq m \leq \ell, T \in \mathcal{T}_h, q \in H^\ell(\Delta_T), \\ \|q - \mathcal{SZ}_h q\|_{m,T} &\leq C_{\mathcal{SZ}} h^{\ell-m} |q|_{\ell,\Delta_T}. \end{aligned}$$

To estimate the second term of Eq. 16, we first calculate an upper bound for $\|\phi_s\|_{1,\Delta_{a_s}}^2$: we have, $\forall s \in \mathcal{T}_{h,\lambda}$,

$$\|\phi_s\|_{1,\Delta_{a_s}}^2 = \sum_{T \in \mathcal{T}_h, T \subset \Delta_{a_s}} \|\phi_s\|_{1,T}^2.$$

Using the technique of passing to a reference element and using the regularity of the mesh \mathcal{T}_h , we obtain that there is a constant $C_{\hat{T}}$ independent of h such that for each $s \in \mathcal{T}_{h,\lambda}$, and for each $T \in \mathcal{T}_h$ with $T \subset \Delta_{a_s}$,

$$\|\phi_s\|_{1,T}^2 \leq \sigma_T C_{\hat{T}} \quad \text{and} \quad \|\phi_s\|_{1,\Delta_{a_s}}^2 \leq \eta \sigma_\Omega C_{\hat{T}},$$

where η is the maximum number of cells of \mathcal{T}_h meeting at a vertex of \mathcal{T}_h (Such a maximum exists because the grid, belonging to a regular family, has a minimum angle size). To control the constants C_s , $s \in \mathcal{T}_{h,\lambda}$, we use Lemma 2 to obtain a lower bound for $\int_s \phi_s|_s$, and we establish an upper bound for $\int_s (\mathcal{SZ}_h p - p)|_s$, using the Cauchy-Schwarz

inequality, Lemma 1 and the estimates for the Scott-Zhang interpolation operator:

$$\begin{aligned} \int_s (\mathcal{SZ}_h p - p)|_s &\leq |s|^{\frac{1}{2}} \|(\mathcal{SZ}_h p - p)|_s\|_{0,s} \\ &\leq C_{\hat{T}}^{\frac{1}{2}} |s|^{\frac{1}{2}} \left\{ \sum_{T \in \mathcal{T}_h; T \cap s \neq \emptyset} \sigma_T \left(h_T^{-1} \|\mathcal{SZ}_h p - p\|_{0,T}^2 + h_T \|\mathcal{SZ}_h p - p\|_{1,T}^2 \right) \right\}^{\frac{1}{2}} \\ &\leq C_{\hat{T}}^{\frac{1}{2}} |s|^{\frac{1}{2}} \sigma_\Omega^{\frac{1}{2}} \left\{ \sum_{T \in \mathcal{T}_h; T \cap s \neq \emptyset} 2C_{\mathcal{SZ}}^2 h |p|_{1,\Delta_T}^2 \right\}^{\frac{1}{2}} \\ &\leq \sqrt{2} C_{\mathcal{SZ}} h^{\frac{1}{2}} C_{\hat{T}}^{\frac{1}{2}} |s|^{\frac{1}{2}} \sigma_\Omega^{\frac{1}{2}} \left\{ \sum_{T \in \mathcal{T}_h; T \cap s \neq \emptyset} |p|_{1,\Delta_T}^2 \right\}^{\frac{1}{2}}. \end{aligned}$$

We thus have

$$\begin{aligned} \sum_{s \in \mathcal{T}_{h,\lambda}} |C_s|^2 \|\phi_s\|_{1,\Delta_{a_s}}^2 &\leq \eta \sigma_\Omega C_{\hat{T}} \sum_{s \in \mathcal{T}_{h,\lambda}} |C_s|^2 \\ &\leq \eta \sigma_\Omega C_{\hat{T}} \sum_{s \in \mathcal{T}_{h,\lambda}} \frac{1}{C_\phi^2 h^2} \left\{ \int_s (\mathcal{SZ}_h p - p)|_s \right\}^2 \\ &\leq \eta \sigma_\Omega^2 C_{\hat{T}} \frac{1}{C_\phi^2 h^2} 2C_{\mathcal{SZ}}^2 h C_\tau \sum_{s \in \mathcal{T}_{h,\lambda}} |s| \left(\sum_{T \in \mathcal{T}_h; T \cap s \neq \emptyset} |p|_{1,\Delta_T}^2 \right) \\ &\leq \eta \sigma_\Omega^2 C_{\hat{T}} \frac{1}{C_\phi^2 h^2} 2C_{\mathcal{SZ}}^2 h C_\tau L h \sum_{s \in \mathcal{T}_{h,\lambda}} \left(\sum_{T \in \mathcal{T}_h; T \cap s \neq \emptyset} |p|_{1,\Delta_T}^2 \right) \\ &\leq 2\eta \sigma_\Omega^2 C_{\hat{T}} \frac{1}{C_\phi^2} C_{\mathcal{SZ}}^2 C_\tau L \tilde{\eta} |p|_{1,\Omega}^2 \\ &= C_1^2 |p|_{1,\Omega}^2, \end{aligned}$$

where $\tilde{\eta} = \sup_{T \in \mathcal{T}_h} \tilde{\eta}_T$ with $\tilde{\eta}_T$ the cardinality of $\{(s, T') \in \mathcal{T}_{h,\lambda} \times \mathcal{T}_h : s \cap T' \neq \emptyset \text{ and } T \subset \Delta_{T'}\}$. Thus, one obtains

$$\|\Pi_h p\|_{1,\Omega} \leq (C_{\mathcal{SZ}} + C_1) \|p\|_{1,\Omega},$$

and Condition 1 is satisfied with $C_\Pi = C_{\mathcal{SZ}} + C_1$. \square

Remark 5 We have supposed that \mathcal{T}_h is uniformly regular. In fact, we only need uniform regularity in a narrow strip containing γ .

In light of Brezzi’s theory for mixed methods [14, 20, 54], the following theorem is an immediate consequence of Lemma 3:

Theorem 2 *Assume that Λ_h is defined by Eq. 12 and that Hypotheses 1 and 2 concerning the meshes \mathcal{T}_h and $\mathcal{T}_{h,\lambda}$ hold. Then there exists a unique solution $(p_h, p_{\gamma,h}; \lambda_h) \in \mathbf{V}_h \times \Lambda_h$ to the discrete, Lagrange-multiplier,*

fracture problem (11). Moreover, there exists a constant C independent of $h, h_\lambda,$ and h_γ such that

$$\begin{aligned} & \|p - p_h\|_{1,\Omega} + \|p_\gamma - p_{\gamma,h}\|_{1,\gamma} + \|\lambda - \lambda_h\|_{-\frac{1}{2},\gamma} \\ & \leq C \left(\inf_{q_h \in V_{h,\Omega}} \|p - q_h\|_{1,\Omega} + \inf_{q_{\gamma,h} \in V_{h,\gamma}} \|p_\gamma - q_{\gamma,h}\|_{1,\gamma} \right. \\ & \quad \left. + \inf_{\mu_h \in \Lambda_h} \|\lambda - \mu_h\|_{-\frac{1}{2},\gamma} \right). \end{aligned} \tag{17}$$

To obtain a convergence estimate, it remains to use approximation results. These are standard for p and p_γ . For λ , we can use the result of [35, Lemma 7]: there exists C_L independent of h_λ such that for all $\mu \in H^{\tilde{\alpha}}(\gamma)$ for $\tilde{\alpha} \in \{0, \frac{1}{2}\}$, we have

$$\inf_{\mu_h \in \Lambda_h} \|\mu - \mu_h\|_{-\frac{1}{2},\gamma} \leq C_L h_\lambda^{\frac{1}{2} + \tilde{\alpha}} \inf_{\mu_h \in \Lambda_h} \|\mu - \mu_h\|_{\tilde{\alpha},\gamma}.$$

Theorem 3 Assume that the hypotheses of Theorem 2 hold. Let $(p, p_\gamma; \lambda) \in \mathbf{V} \times \Lambda$ be the solution to Problem (9), and $(p_h, p_{\gamma,h}; \lambda_h) \in \mathbf{V}_h \times \Lambda_h$ be the solution to Problem (11). Assume that (p, p_γ) belongs to $H^\alpha(\Omega) \times H^2(\gamma)$ for an $\alpha \in [\frac{3}{2} - \varepsilon, 2]$ ($\varepsilon > 0$), and that λ belongs to $H^{\tilde{\alpha}}(\gamma)$ for some $\tilde{\alpha} \in [0, \frac{1}{2}]$. Then, there exists a constant C independent of $h, h_\lambda,$ and h_γ such that

$$\begin{aligned} & \|p - p_h\|_{1,\Omega} + \|p_\gamma - p_{\gamma,h}\|_{1,\gamma} + \|\lambda - \lambda_h\|_{-\frac{1}{2},\gamma} \\ & \leq C \left(h^{\alpha-1} \|p\|_{\alpha,\Omega} + h_\gamma \|p_\gamma\|_{2,\gamma} + h_\lambda^{\frac{1}{2} + \tilde{\alpha}} \|\lambda\|_{\tilde{\alpha},\gamma} \right). \end{aligned} \tag{18}$$

Thus, depending on the regularity of the continuous solution, one expects a convergence rate of order between $h^{\frac{1}{2} - \varepsilon}$ and h . In all of the numerical experiments that we have examined, we obtained an order of at least h for the variables p_h and $p_{\gamma,h}$ and an order between $h^{\frac{1}{2}}$ and h for λ_h : cf. Figs. 5, 7, and 10.

3.3 An alternative Lagrange multiplier space with continuous, piecewise-linear multipliers

The study in this subsection is motivated by the idea that for some alternative, discrete, Lagrange-multiplier space, it might be possible to use a relation between the Lagrange multiplier space and the fracture pressure space to establish a discrete inf-sup condition. Here, we consider the simplest possible such case: the case in which the spaces $V_{h,\Omega}$ and $V_{h,\gamma}$ are still defined by Eq. 10, but the fracture meshes are equal, $\mathcal{T}_{h,\lambda} = \mathcal{T}_{h,\gamma}$, and indeed (12) is replaced by

$$\Lambda_h = V_{h,\gamma}. \tag{19}$$

Proposition 1 Assume that Λ_h is defined by Eq. 19 and that $\mathcal{T}_{h,\lambda} = \mathcal{T}_{h,\gamma}$ is uniformly regular. Then there exists a

unique solution $(p_h, p_{\gamma,h}; \lambda_h) \in \mathbf{V}_h \times \Lambda_h$ to the discrete, Lagrange-multiplier, fracture problem (11).

Proof We show that the discrete inf-sup condition is satisfied by the operator $b(\cdot, \cdot; \cdot)$ on $\mathbf{V}_h \times \Lambda_h$, using the norm $\|\cdot\|_{\mathbf{V}}$ for \mathbf{V}_h and for Λ_h the discrete norm defined for $\mu_h \in \Lambda_h$ by

$$\|\mu_h\|_{\Lambda_h} = \|\mu_h\|_{-\frac{1}{2},h_\lambda,\gamma} = h_\lambda^{\frac{1}{2}} \|\mu_h\|_{0,\gamma}. \tag{20}$$

Let $\lambda_h \in \Lambda_h$. As $\Lambda_h = V_{h,\gamma}$, we take $r_{h,\gamma} = -\lambda_h$ and $r_h = 0$. Then we have

$$b(r_h, r_{h,\gamma}; \lambda_h) = b(0, -\lambda_h; \lambda_h) = \|\lambda_h\|_{0,\gamma}^2$$

Using the uniform regularity of the mesh $\mathcal{T}_{h,\lambda} = \mathcal{T}_{h,\gamma}$, and using an inverse inequality [24, Corollary 1.141, page 76 or Remark 1.143 (i), page 77], there is a constant $\hat{\theta}$ such that

$$\begin{aligned} \|(r_h, r_{h,\gamma})\|_{\mathbf{V}} \|\lambda_h\|_{\Lambda_h} &= \|\lambda_h\|_{1,\gamma} \|\lambda_h\|_{-\frac{1}{2},h_\lambda,\gamma} \\ &= \|\lambda_h\|_{1,\gamma} h_\lambda^{\frac{1}{2}} \|\lambda_h\|_{0,\gamma} \\ &\leq \hat{\theta} h_\lambda^{-\frac{1}{2}} \|\lambda_h\|_{0,\gamma}^2 \\ &\leq \hat{\theta} h_\lambda^{-\frac{1}{2}} b(r_h, r_{h,\gamma}; \lambda_h). \end{aligned}$$

Thus, the discrete inf-sup condition is satisfied with a constant $\theta_h = \hat{\theta}^{-1} h_\lambda^{\frac{1}{2}}$ which is not independent of h_λ . \square

Remark 6 Note that there is no compatibility condition on the meshes \mathcal{T}_h and $\mathcal{T}_{h,\lambda} = \mathcal{T}_{h,\gamma}$ in the proof, neither does \mathcal{T}_h need to be uniformly regular. In particular, there is no hypothesis on the respective mesh sizes h and $h_\lambda = h_\gamma$. However, with this choice of Λ_h , the discrete inf-sup condition is not uniform in h_λ , so one can assure a unique solution but not convergence. We remark that the numerical results of Section 4 show good convergence rates even for this choice of Λ_h ; cf. Figs. 5, 7, and 11.

4 Numerical results

The emphasis of this section is on numerical experiments using the two different discretizations presented in Section 3. In particular, the mesh size of the discrete multipliers h_λ and its impact on accuracy and convergence will be addressed. We recall that the two discretizations of the continuous problem (9) vary only in the way the Lagrange multiplier is defined. By $\lambda_h|_s \in \mathbb{P}^0(s)$, cf. Eq. 12, we refer to the discretization of Section 3.2 and by $\lambda_h|_s \in \mathbb{P}^1(s)$, cf. Eq. 19, to the discretization of Section 3.3. The latter implies that $h_\lambda = h_\gamma$. In the former case, we consider $h_\lambda \approx 2h$, in order to show that the condition $h_\lambda > 3h$ (see Remark 1) is sufficient but probably too restrictive in practice. Due to the higher permeability in the fracture, which may demand higher accuracy at the fracture interface, in all cases we have

taken $h_\gamma \leq h$. With the above choices of h_λ , we ensure that $h_\lambda \geq \min\{h, h_\gamma\}$, to prevent a poorly conditioned system matrix.

We analyze the performance of the proposed method by means of several test cases of different complexity. Based on an oblique fracture extending up to the boundaries of the matrix domain and an internal fracture with a junction and with fracture tips in the interior of the matrix, we study the numerical convergence of the method in Section 4.1 and Section 4.2, respectively. These examples are followed by more complex test cases with a regular fracture network in Section 4.3 and a more realistic benchmark problem in Section 4.4. The accuracy and convergence are validated by means of a comparison with other methods in this field [28].

As the fracture interface is generally not aligned with the matrix mesh, we use a sufficiently fine reference solution for the computation of the error in all examples. In the simplified case of a conforming fracture, i.e., aligned with the matrix mesh, we obtain optimal rates of convergence in the matrix as well as in the fracture (results not shown here, see [43]; cf. also [44]). A direct solver was used to solve the linear systems.

4.1 Case 1: an oblique fracture

The first setup is a two-dimensional, square domain $\Omega := [0, 1]^2$ with homogeneous Neumann conditions on the horizontal boundaries and nonhomogeneous Dirichlet conditions on the vertical boundaries ($p = 1$ on the left and $p = 4$ on the right). An oblique fracture γ with $\mathbf{K}_\gamma = 10\mathbf{I}_\gamma$, $\mathbf{K} = \mathbf{I}$, extends from the left to the right part of the horizontal boundaries of the matrix domain Ω with Dirichlet boundary values $p_\gamma = 1$ on the lower tip and $p_\gamma = 4$ on the upper tip. The test case and the pressure distribution are shown in Fig. 4. Because of the geometry of the setup, the oblique fracture mesh is not aligned with the rectangular elements of the matrix grid (nonconforming).

Figure 5 displays the numerical convergence analysis of the primary variables in different norms for $h \in \{1/8, 1/16, \dots, 1/128\}$ based on a reference solution computed with a resolution of $h = 1/512$. The mesh size of the fracture h_γ is always half of the matrix mesh size, i.e., $h_\gamma \approx h/2$.

The results in Fig. 5 are in accordance with or better than the theoretical findings: the H^1 errors for fracture and matrix pressures converge linearly independent of the utilized discretization of the Lagrange multiplier and the Lagrange multiplier converges with rates up to $O(h_\lambda)$ in the discrete norm $\|\cdot\|_{-\frac{1}{2}, h_\lambda, \gamma}$ defined in Eq. 20. The Lagrange multiplier error remains at quite high levels, but this does not degrade the error for p or p_γ which are the more relevant physical unknowns. In the L^2 norm, the

errors for the matrix pressure converge linearly, and the errors for the fracture pressure converge with rates between $O(h_\gamma^{\frac{3}{2}})$ and $O(h_\gamma^2)$. Additional numerical experiments (not presented here) showed that it is possible to use a more refined fracture mesh, e.g., $h_\gamma \approx h/10$, with conclusions in no way significantly different from those above. The only difference is an improvement in the fracture pressure error.

We conclude that in the present test case with an oblique fracture, the choice of the ansatz functions of the Lagrange multiplier does not affect the rates of convergence and the errors significantly. The major difference in Fig. 5 stems from the choice of the mesh sizes.

Remark 7 When h_λ is too small (typically $h_\lambda < h/2$), Hypotheses 1 and 2 are not satisfied by far, and problem (11) is not stable. This is characterized by solvability issues of the linear system (at least a very poor conditioning of the matrix) [43].

4.2 Case 2: a y-shaped fracture

The next setup rests upon a slightly different fracture-matrix scenario with fracture tips ending within the matrix domain Ω . In contrast to the test case of the previous Section 4.1, a y-shaped fracture splitting into two parts is located in the center of the domain. We impose no flow conditions at the fracture tips. The test case and the pressure distribution are shown in Fig. 6.

The numerical convergence study in different norms is displayed in Fig. 7 for $h \in \{1/8, 1/16, \dots, 1/128\}$ based on a reference solution computed with resolution $h = 1/512$.

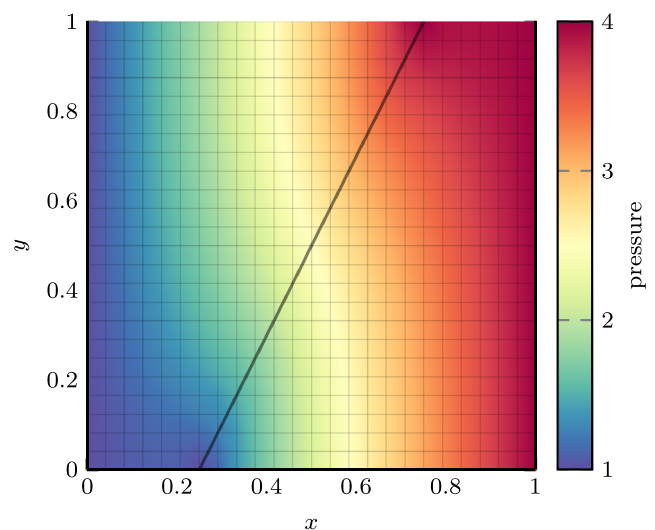


Fig. 4 Case 1 (an oblique fracture): Pressure distribution of a simulation with $h = 1/24$, $h_\lambda = h_\gamma = 1/48$, $\lambda_h|_s \in \mathbb{P}^1(s)$

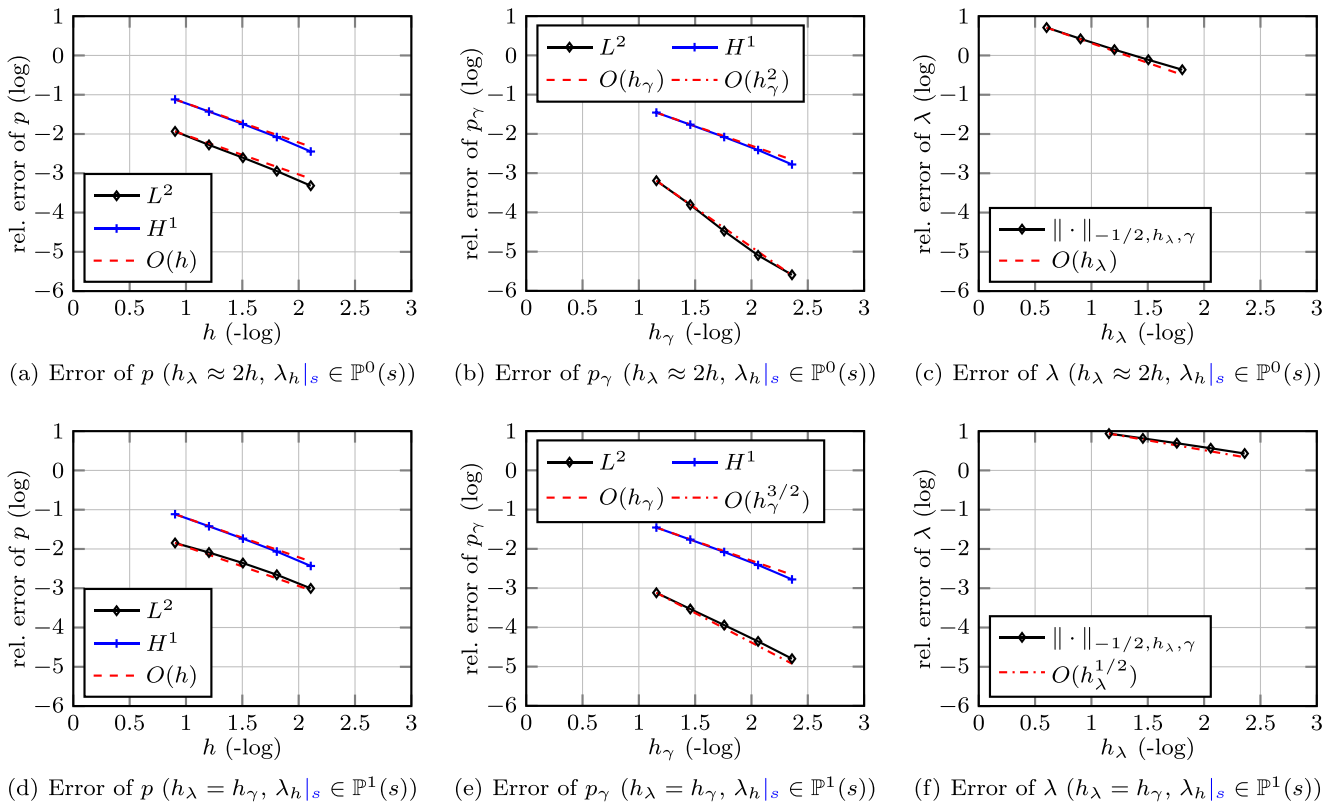


Fig. 5 Case 1 (an oblique fracture): Convergence of matrix pressure p , fracture pressure p_γ , and Lagrange multiplier λ for $h_\lambda \approx 2h, \lambda_h|_s \in \mathbb{P}^0(s)$ (above) and for $h_\lambda = h_\gamma, \lambda_h|_s \in \mathbb{P}^1(s)$ (below) depending on the mesh size

Apart from a small kink in Fig. 7b the linear rate of convergence of the H^1 error observed in the previous example (cf. Fig. 5) is maintained. The L^2 errors have approximately linear convergence with slightly improved rates of the matrix in the case $h_\lambda \approx 2h, \lambda_h|_s \in \mathbb{P}^0(s)$.

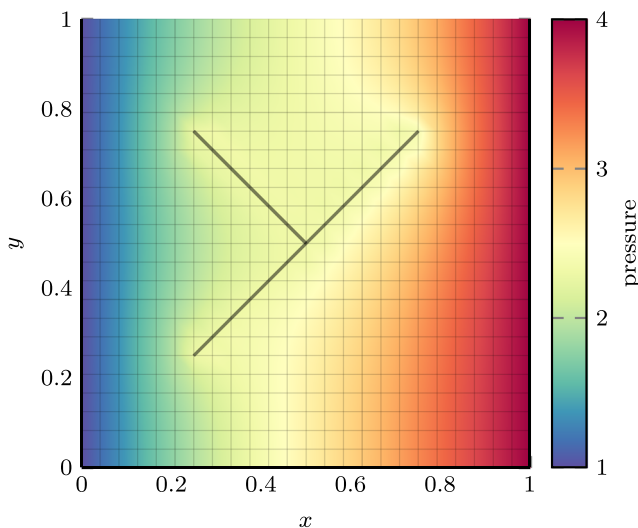


Fig. 6 Case 2 (a y-shaped fracture): Pressure distribution of a simulation with $h = 1/24, h_\lambda = h_\gamma = 1/48, \lambda_h|_s \in \mathbb{P}^1(s)$

It is worth noticing that the difference of L^2 and H^1 error in the fracture is marginal. The absolute value of the L^2 errors is higher compared to those of Fig. 5. The errors of the Lagrange multiplier are in the range of $O(h_\lambda^{1/2})$ and $O(h_\lambda^{3/4})$. Again, additional numerical experiments show that it is possible to use a more refined fracture mesh, e.g., $h_\gamma \approx h/10$, with roughly the same conclusions.

We conclude that in this case of a splitting and internal fracture, the choice of the ansatz function of the discrete Lagrange multipliers has a stronger impact on the convergence rates. Nonetheless, the numerical experiments indicate the overall convergence. The junction of the fracture lines and the fracture tips ending within the matrix domain may additionally reduce the regularity of the solution. This may explain why the choice of the ratio of the involved mesh sizes becomes more important.

4.3 Case 3: a fracture network

The third setup is a more complex test case with a regular fracture network presented in [33] but with boundary conditions slightly modified (in accordance with [28]). On the horizontal boundaries, homogeneous Neumann conditions are imposed. Moreover, we impose nonhomogeneous Neumann conditions (inflow) on the left

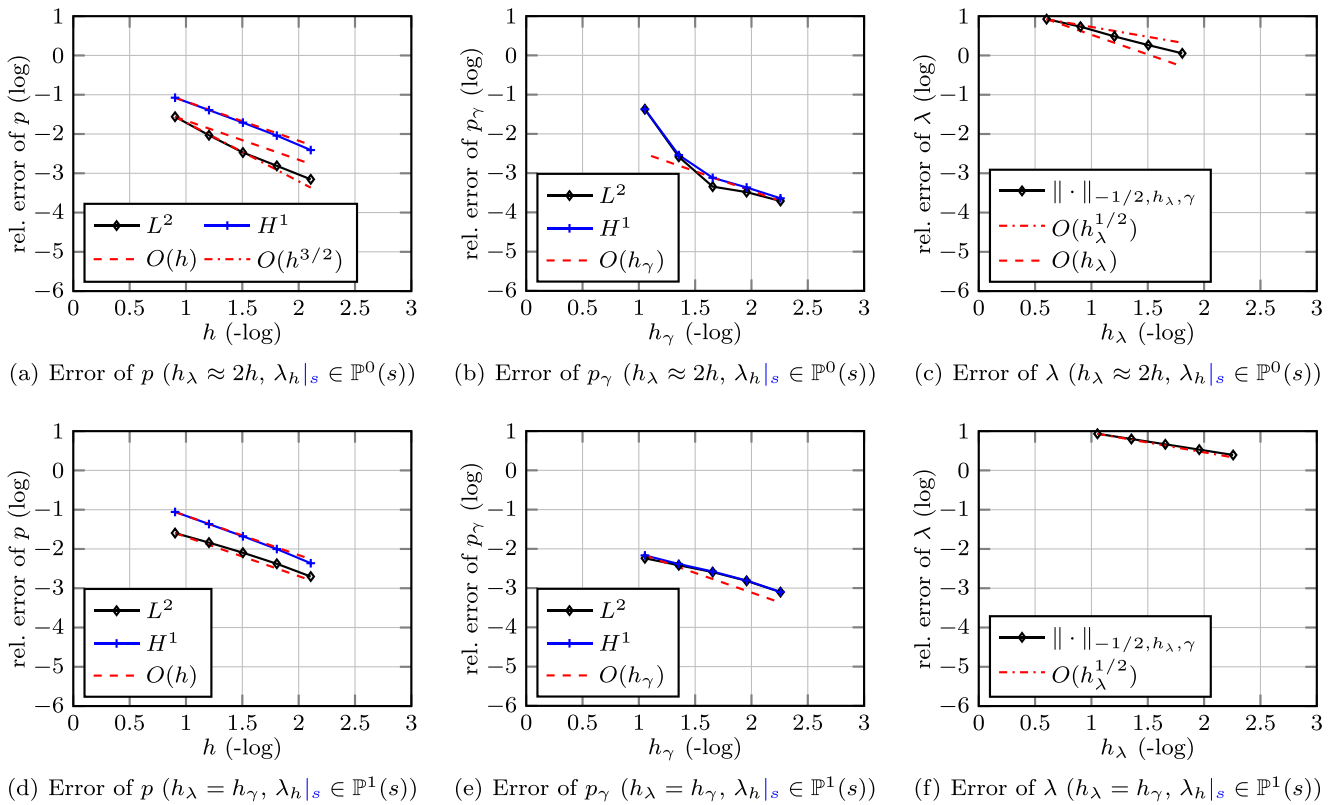


Fig. 7 Case 2 (a y-shaped fracture): Convergence of matrix pressure p , fracture pressure p_γ , and Lagrange multiplier λ for $h_\lambda \approx 2h, \lambda_h|_s \in \mathbb{P}^0(s)$ (above) and for $h_\lambda = h_\gamma, \lambda_h|_s \in \mathbb{P}^1(s)$ (below) depending on the mesh size

and nonhomogeneous Dirichlet boundary conditions on the right.

All fractures of the test case have the uniform aperture $d = 10^{-4}$. The matrix domain is characterized by a

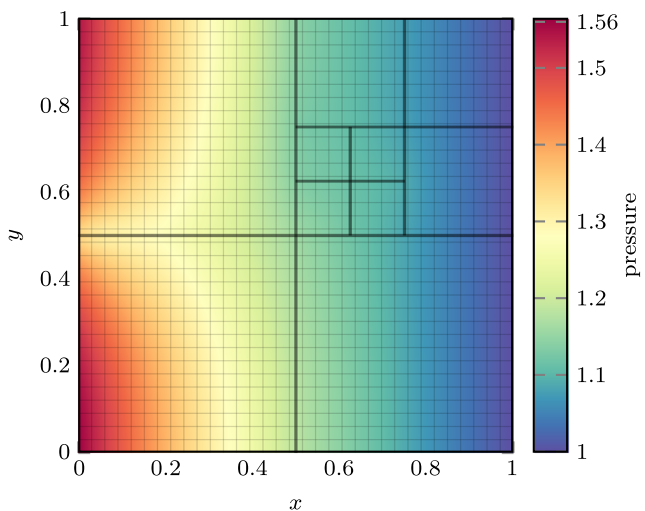


Fig. 8 Case 3 (a fracture network): Pressure distribution of simulation with $h = 1/33, h_\gamma = 1/32, h_\lambda \approx 2h, \lambda_h|_s \in \mathbb{P}^0(s)$. The fracture network is shown in black

permeability of $\mathbf{K} = \mathbf{I}$ and the fracture by a permeability of $\mathbf{K}_\gamma = \mathbf{I}_\gamma$. Note that the aperture of the fracture is incorporated in the value of \mathbf{K}_γ and the inflow condition $\mathbf{u}_\gamma \cdot \mathbf{n}_\gamma$ on the left boundary. The resulting pressure distribution of a simulation with nonconforming configuration and $h = 1/33, h_\gamma = 1/32, h_\lambda \approx 2h, \lambda_h|_s \in \mathbb{P}^0(s)$ is shown in Fig. 8.

Based on the benchmark study [28], we compare the proposed Lagrange-multiplier method with several other available methods in the field of single-phase flow in fractured porous media. The reference solution used here is computed with a mimetic finite difference method [21] using a two-dimensional grid in the fracture and the matrix domain. The interested reader is referred to [28] for further details of the different methods. Figure 9 displays the comparison of the pressure profile at $y = 0.7$ and $x = 0.5$, where the proposed method of this work is denoted by LM-FEM, (Lagrange multiplier - finite element method). Figure 9 shows that the distribution of the pressure is in good agreement with the other methods. With 1089 rectangular elements in the matrix and 112 segments in the fracture, the simulation of the Lagrange multiplier method is in the same range of numbers of elements as the other methods. Similarly, the L^2 error in the matrix $err_m =$

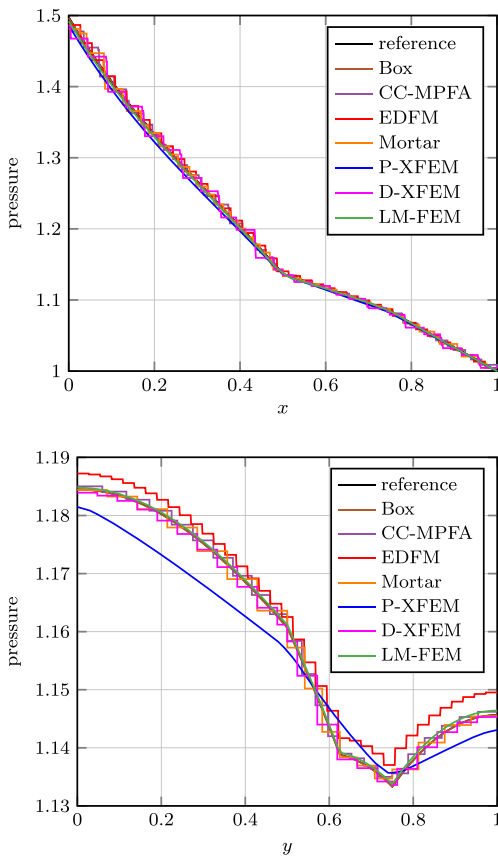


Fig. 9 Case 3 (a fracture network): Comparison with other methods, cf. [28], at $y = 0.7$ (above) and $x = 0.5$ (below). Lagrange multiplier method (with $\lambda_h|_s \in \mathbb{P}^0(s)$, $h = 1/33$, $h_\gamma = 1/32$, $h_\lambda \approx 2h$ and nonconforming grid) denoted by LM-FEM

$1.0 \cdot 10^{-2}$ and in the fracture $err_\gamma = 6.5 \cdot 10^{-3}$ is in the same range.

Building on this configuration, the meshes are consecutively refined three times by a factor of two ($h \in \{1/33, 1/65, 1/129, 1/257\}$) in order to investigate the convergence in a similar way as proposed in [28]. The resulting convergence study of both, matrix and fracture pressure, is illustrated in Fig. 10. Again, the Lagrange multiplier method is characterized by a similar convergence behavior as the other methods of the benchmark, with linear convergence rates in the matrix and the fracture. Additional numerical experiments indicated linear rates of convergence also for different discretizations such as $\lambda_h|_s \in \mathbb{P}^1(s)$, $h_\lambda = h_\gamma$ or a refined fracture mesh as long as the mesh of the multiplier is not chosen too small compared to the matrix mesh, e.g., $h_\lambda \geq h/2$.

The numerical results demonstrate that in practice, the mesh size of the Lagrange multiplier can be chosen smaller than the theoretical results of Section 3 suggest. Moreover, the results show that the multiplier method is able to compete with other DFM models in the field.

4.4 Case 4: the hydrocoin benchmark

The last setup is a more realistic flow problem of the international hydrocoin project [58]. The benchmark accounts for the morphology of the geological formation and is characterized by the piezometric head and hydraulic conductivities. It comprises two conductive and intersecting fractures with different aperture, $d_1 \approx 7.07 \text{ m}$ and $d_2 \approx 14.76 \text{ m}$, and uniform hydraulic conductivity 10^{-6} m/s . The surrounding matrix rock has an isotropic hydraulic conductivity of 10^{-8} m/s . The surface elevation represents the Dirichlet boundary condition at the top of the domain. No-flow Neumann boundary conditions are imposed on the other boundaries. Note that we slightly modified the original domain as in [28] in order to preserve the comparability between different fracture models. The plot at the top of Fig. 11 shows the distribution of the piezometric head of a simulation with $h \approx 34\text{m}$, $h_\gamma = h_\lambda \approx h/2$, $\lambda_h|_s \in \mathbb{P}^1(s)$.

A comparison with other fracture models at a depth of 200m based on [28] is shown in the plot at the bottom of Fig. 11. The reference solution used here is again computed with a mimetic finite difference method [21]

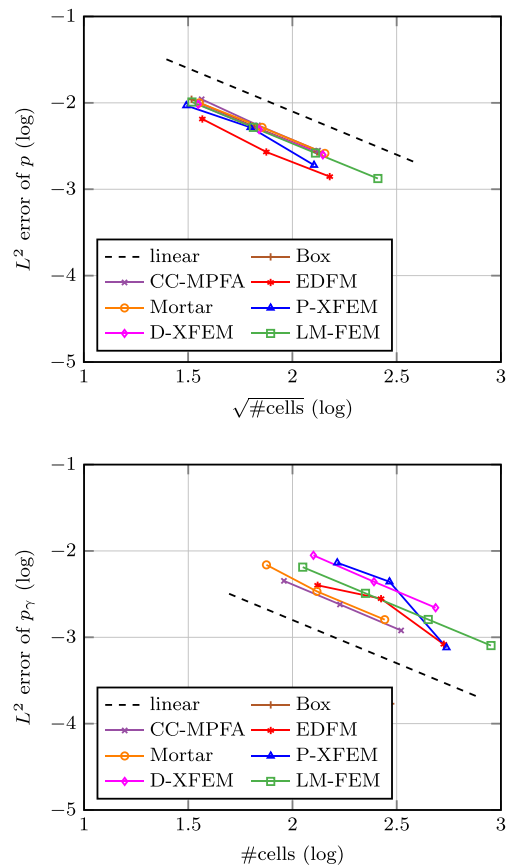


Fig. 10 Case 3 (a fracture network): Convergence of matrix pressure p (above) and fracture pressure p_γ (below) for $h_\lambda \approx 2h$, $\lambda_h|_s \in \mathbb{P}^0(s)$ depending on the number of elements compared to other methods, cf. [28]. Lagrange multiplier method denoted by LM-FEM

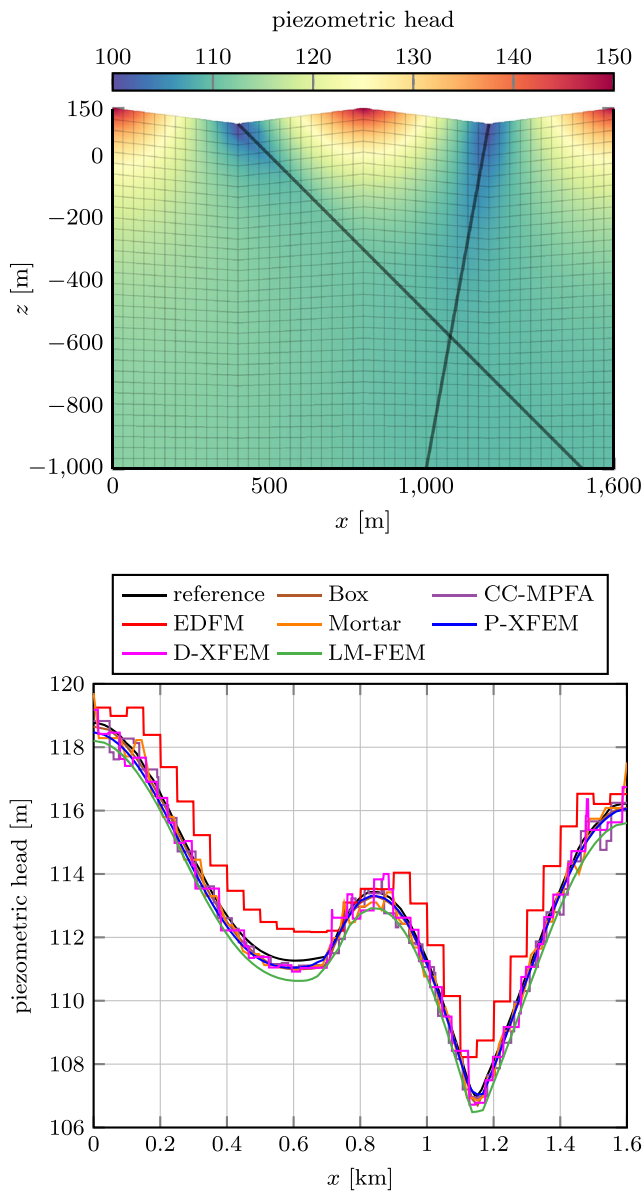


Fig. 11 Case 4 (the hydrocoin benchmark): Nonconforming simulation with $h \approx 34m$, $h_\gamma = h_\lambda \approx h/2$, $\lambda_h|_s \in \mathbb{P}^1(s)$ (above) and comparison with other methods, cf. [28], at $z = -200m$ (below). Lagrange multiplier method denoted by LM-FEM

using a two-dimensional grid in the fracture and in the matrix domain. Figure 11 indicates that the approximation with the proposed method stays within the range of the compared distributions of the hydraulic head. The global error in the matrix $err_m = 1.6 \cdot 10^{-2}$ and the fracture error $err_\gamma = 1.3 \cdot 10^{-2}$ are slightly higher than those of the other methods. Additional simulations with piecewise constant multipliers $\lambda_h|_s \in \mathbb{P}^0(s)$ showed that the errors increase rapidly with the coarsening of the multiplier mesh. However, a more refined fracture mesh does not affect the results significantly.

A more detailed convergence study was not performed in this case since the large width of the fractures raises the question if the equidimensional mimetic finite difference solution is a precise reference solution to reduced models of co-dimension one.

5 Conclusion

We presented a novel approach to modeling single-phase, single-component, Darcy flow in fractured porous media based on the use of a Lagrange multiplier, which couples the flow in the fracture with that in the surrounding matrix, and showed that there exists a unique solution to the primal formulation of the continuous problem. In particular, this method allows for the use of a mesh in the matrix domain that is not aligned with the fracture. In order to approximate the fracture and the matrix pressure of the interface model, two different types of finite element discretizations were studied. Both discretizations are based on a discrete multiplier space defined on the fracture interface. However, they differ in the choice of the mesh and the basis functions of the Lagrange multiplier.

The first of these relies on discontinuous piecewise constant basis functions on sufficiently large multiplier elements ($h_\gamma \geq 3h$). Under this condition, following [35], we proved existence, uniqueness, and convergence of the discrete problem. Several numerical experiments confirmed the theoretical results and validated the approach. The numerical experiments showed that in practice, the mesh size of the multiplier can be chosen finer than the theoretical results suggest. Provided that $h_\lambda \geq \min\{h, h_\gamma\}$, a multiplier mesh size in the range of the matrix element, i.e., $h_\lambda \approx h$, yields a reasonable balance between accuracy, convergence, and conditioning.

The second discretization is based on continuous, piecewise-affine, multiplier elements. In particular, the mesh for the multiplier is the same as that for the fracture. In this case, we could prove that there exists a unique solution of the discrete problem, but not convergence. However, the numerical results indicated that the discrete problem converges to the reference solution and validated the approach. Similar to the previous discretization, mesh sizes of $h_\lambda = h_\gamma \approx h$ or $h_\lambda = h_\gamma \approx h/2$ yield a reasonable balance between accuracy and convergence. We note though that the condition number is generally significantly higher for the second discretization for λ_h (\mathbb{P}^1) than for the first (\mathbb{P}^0).

The numerical examples showed that the errors of matrix and fracture pressure decrease linearly in the H^1 norm. However, the errors deviate from the desired rates in the L^2 norm resulting from the nonconforming fashion the fracture intersects the matrix elements and the regularity

of the different test cases. Therefore, the L^2 -convergence generally varies between $O(h)$ and $O(h^2)$. If the fracture mesh is aligned with the matrix mesh, we obtain optimal rates of convergence. In accordance with the theoretical findings, the Lagrange multiplier is characterized by rates up to $O(h_\lambda)$. The results of the benchmark problems in [28] lead us to the conclusion that the method is in good agreement with other fracture models and is an efficient alternative for the approximation of flow problems in fractured porous media.

Funding information The authors received financial support from the German Research Foundation (DFG) for the project within the Cluster of Excellence in Simulation Technology (EXC 310/2) at the University of Stuttgart.

References

- Ahmed, E., Jaffré, J., Roberts, J.E.: A reduced fracture model for two-phase flow with different rock types. *Math. Comput. Simul.* **137**, 49–70 (2017)
- Ahmed, R., Edwards, M.G., Lamine, S., Huisman, B.A.H., Pal, M.: Control-volume distributed multi-point flux approximation coupled with a lower-dimensional fracture model. *J. Comput. Phys.* **284**, 462–489 (2015)
- Ahmed, R., Edwards, M.G., Lamine, S., Huisman, B.A.H., Pal, M.: Three-dimensional control-volume distributed multi-point flux approximation coupled with a lower-dimensional surface fracture model. *J. Comput. Phys.* **303**, 470–497 (2015)
- Ainsworth, M.: A posteriori error estimation for discontinuous Galerkin finite element approximation. *SIAM J. Numer. Anal.* **45**(4), 1777–1798 (2007)
- Alboin, C., Jaffré, J., Roberts, J.E.: Domain decomposition for flow in porous media with fractures. In: *Domain Decomposition Methods in Sciences and Engineering*. Domain Decomposition Press (1999)
- Alboin, C., Jaffré, J., Roberts, J.E., Serres, C.: Modeling fractures as interfaces for flow and transport in porous media. In: *Fluid Flow and Transport in Porous Media: Mathematical and Numerical Treatment*, Contemp. Math., vol. 295, pp. 13–24. Amer. Math. Soc., Providence (2002)
- Angot, P., Boyer, F., Hubert, F.: Numerical modelling of flow in fractured porous media. In: *FVCA IV*, pp. 249–260. ISTE, London (2005)
- Antonietti, P.F., Facciola, C., Russo, A., Verani, M.: Discontinuous Galerkin approximation of flows in fractured porous media. *Tech. Rep. 22/2016 Politecnico di Milano* (2016)
- Antonietti, P.F., Formaggia, L., Scotti, A., Verani, M., Verzott, N.: Mimetic finite difference approximation of flows in fractured porous media. *ESAIM: M2AN* **50**(3), 809–832 (2016)
- Baca, R.G., Arnett, R.C., Langford, D.W.: Modelling fluid flow in fractured-porous rock masses by finite-element techniques. *Int. J. Numer. Methods Fluids* **4**, 337–348 (1984)
- Berkowitz, B.: Characterizing flow and transport in fractured geological media: A review. *Adv. Water Resour.* **25**(8–12), 861–884 (2002)
- Berrone, S., Canuto, C., Pieraccini, S., Scialò, S.: Uncertainty quantification in discrete fracture network models: stochastic fracture transmissivity. *Comput. Math. Appl.* **70**(4), 603–623 (2015)
- Berrone, S., Pieraccini, S., Scialò, S.: An optimization approach for large scale simulations of discrete fracture network flows. *J. Comput. Phys.* **256**, 838–853 (2014)
- Boffi, D., Brezzi, F., Fortin, M.: *Mixed finite element methods and applications*. Springer Series in Computational Mathematics, vol. 44. Springer, Heidelberg (2013)
- Boon, W., Nordbotten, J., Yotov, I.: Robust discretization of flow in fractured porous media. *SIAM J. Numer. Anal.* **56**(4), 2203–2233 (2018)
- Brenner, K., Groza, M., Guichard, C., Lebeau, G., Masson, R.: Gradient discretization of hybrid dimensional Darcy flows in fractured porous media. *Numer. Math.* **134**(3), 569–609 (2016)
- Brenner, K., Groza, M., Guichard, C., Masson, R.: Vertex approximate gradient scheme for hybrid dimensional two-phase Darcy flows in fractured porous media. *ESAIM Math. Model. Numer. Anal.* **49**(2), 303–330 (2015)
- Brenner, K., Groza, M., Jeannin, L., Masson, R., Pellerin, J.: Immiscible two-phase Darcy flow model accounting for vanishing and discontinuous capillary pressures: application to the flow in fractured porous media. *Comput Geosci* (2017)
- Brenner, S.C., Scott, L.R.: *The mathematical theory of finite element methods*. Texts in Applied Mathematics. Springer, New York (2002)
- Brezzi, F.: On the existence, uniqueness and approximation of saddle-point problems arising from Lagrangian multipliers. *RAIRO Anal. Numer.* **2**(10), 129–151 (1974)
- Brezzi, F., Lipnikov, K., Simoncini, V.: A family of mimetic finite difference methods on polygonal and polyhedral meshes. *Math. Models Methods Appl. Sci* **15**(10), 1533–1551 (2005)
- Capatina, D., Luce, R., El-Otmany, H., Barrau, N.: Nitsche’s extended finite element method for a fracture model in porous media. *Appl. Anal.* **95**(10), 2224–2242 (2016)
- D’Angelo, C., Scotti, A.: A mixed finite element method for Darcy flow in fractured porous media with non-matching grids. *ESAIM: Math. Model. Numer. Anal.* **46**(2), 465–489 (2012)
- Ern, A., Guermond, J.L.: *Theory and practice of finite elements*. Applied Mathematical Sciences, vol. 159. Springer, New York (2004)
- Ern, A., Guermond, J.L.: *Finite elements I: basic theory and practice*. To appear in Springer-Verlag, New York (2018)
- Faille, I., Flauraud, E., Nataf, F., Pegaz-Fiornet, S., Schneider, F., Willien, F.: A new fault model in geological basin modelling, application to finite volume scheme and domain decomposition methods. In: *FVCA III*, pp. 543–550. Hermès Penton Sci (2002)
- Faille, I., Fumagalli, A., Jaffré, J., Roberts, J.E.: Model reduction and discretization using hybrid finite volumes for flow in porous media containing faults. *Comput. Geosci.* **20**(2), 317–339 (2016)
- Flemisch, B., Berre, I., Boon, W., Fumagalli, A., Schwenck, N., Scotti, A., Stefansson, I., Tatomir, A.: Benchmarks for single-phase flow in fractured porous media. *Adv. Water Resour.* **111**, 239–258 (2018)
- Frih, N., Martin, V., Roberts, J.E., Saada, A.: Modeling fractures as interfaces with nonmatching grids. *Comput. Geosci.* **16**(4), 1043–1060 (2012)
- Frih, N., Roberts, J.E., Saada, A.: Modeling fractures as interfaces: a model for Forchheimer fractures. *Comput. Geosci.* **12**(1), 91–104 (2008)
- Fumagalli, A., Scotti, A.: Numerical modelling of multiphase subsurface flow in the presence of fractures. *Commun. Appl. Ind. Math.* **3**(1), e–380,23 (2012)
- Fumagalli, A., Scotti, A.: A numerical method for two-phase flow in fractured porous media with non-matching grids. *Adv. Water Resour.* **62**, Part C, 454–464 (2013). *Computational Methods in Geologic CO2 Sequestration*

33. Geiger, S., Dentz, M., Neuweiler, I.: A novel multi-rate dual-porosity model for improved simulation of fractured and multi-porosity reservoirs. *Soc. Petrol. Eng. J.* **18**(4), 670–684 (2013)
34. Geiger, S., Matthai, S., Niessner, J., Helmig, R.: Black-oil simulations for three-component, three-phase flow in fractured porous media. *Soc. Petrol. Eng. J.* **14**(2), 338–354 (2009)
35. Girault, V., Glowinski, R.: Error analysis of a fictitious domain method applied to a Dirichlet problem. *Jpn. J. Ind. Appl. Math.* **12**(3), 487 (1995)
36. Gläser, D., Helmig, R., Flemisch, B., Class, H.: A discrete fracture model for two-phase flow in fractured porous media. *Adv. Water Resour.* **110**, 335–348 (2017)
37. Hoteit, H., Firoozabadi, A.: An efficient numerical model for incompressible two-phase flow in fractured media. *Adv. Water Resour.* **31**, 891–905 (2008)
38. Huang, H., Long, T.A., Wan, J., Brown, W.P.: On the use of enriched finite element method to model subsurface features in porous media flow problems. *Comput. Geosci.* **15**(4), 721–736 (2011)
39. Jaffré, J., Mnejja, M., Roberts, J.E.: A discrete fracture model for two-phase flow with matrix-fracture interaction. *Procedia Comput. Sci.* **4**, 967–973 (2011)
40. Karimi-Fard, M., Durlowski, L.J., Aziz, K.: An efficient discrete-fracture model applicable for general-purpose reservoir simulators. *Soc. Petrol. Eng. J.* **9**(2), 227–236 (2004)
41. Karimi-Fard, M., Firoozabadi, A.: Numerical simulation of water injection in 2D fractured media using discrete-fracture model. *SPE Reservoir Eval. Eng.* **4**, 117–126 (2003)
42. Knabner, P., Roberts, J.E.: Mathematical analysis of a discrete fracture model coupling Darcy flow in the matrix with Darcy–Forchheimer flow in the fracture. *ESAIM: Math. Model. Numer. Anal.* **48**(5), 1451–1472 (2014)
43. Köppel, M.: Flow in heterogeneous porous media: fractures and uncertainty quantification. Ph.D. thesis. University of Stuttgart, Germany. ISBN 978-3-8439-3731-3 (2018)
44. Köppel, M., Martin, V., Roberts, J.E.: A stabilized Lagrange multiplier finite-element method for flow in porous media with fractures. submitted (2018). <https://hal.archives-ouvertes.fr/hal-01761591>
45. Lesinigo, M., D’Angelo, C., Quarteroni, A.: A multiscale Darcy–Brinkman model for fluid flow in fractured porous media. *Numer. Math.* **117**(4), 717–752 (2011)
46. List, F., Kumar, K., Pop, I.S., Radu, F.A.: Rigorous upscaling of unsaturated flow in fractured porous media. UHasselt Computational Mathematics Preprint (2018). Nr. UP-18-04
47. Martin, V., Jaffré, J., Roberts, J.E.: Modeling fractures and barriers as interfaces for flow in porous media. *SIAM J. Sci. Comput.* **26**(5), 1667–1691 (2005)
48. Matthai, S.K., Mezentsev, A.A., Belayneh, M.: Finite element/node-centered finite-volume two-phase-flow experiments with fractured rock represented by unstructured hybrid-element meshes. *SPE Reservoir Eval. Eng.*, 10 (2007)
49. Moinfar, A., Varavei, A., Sepehrnoori, K., Johns, R.T.: Development of an efficient embedded discrete fracture model for 3D compositional reservoir simulation in fractured reservoirs. *Soc. Petrol. Eng. J.* (2014)
50. Monteagudo, J.E.P., Firoozabadi, A.: Control-volume method for numerical simulation of two-phase immiscible flow in two- and three-dimensional discrete-fractured media. *Water Resour. Res.* **40**(7), W07405 (2004)
51. Neuman, S.P.: Trends, prospects and challenges in quantifying flow and transport through fractured rocks. *Hydrogeol. J.* **13**(1), 124–147 (2005)
52. Pichot, G., Erhel, J., de Dreuzy, J.R.: A generalized mixed hybrid mortar method for solving flow in stochastic discrete fracture networks. *SIAM J. Sci. Comput.* **34**(1), B86–B105 (2012)
53. Reichenberger, V., Jakobs, H., Bastian, P., Helmig, R.: A mixed-dimensional finite volume method for two-phase flow in fractured porous media. *Adv. Water Resour.* **29**(7), 1020–1036 (2006)
54. Roberts, J.E., Thomas, J.M.: Mixed and hybrid methods. In: *Handbook of Numerical Analysis*, vol. II, pp. 523–639. *Handb. Numer. Anal.*, North-Holland (1991)
55. Sandve, T.H., Berre, I., Nordbotten, J.M.: An efficient multi-point flux approximation method for discrete fracture–matrix simulations. *J. Comput. Phys.* **231**(9), 3784–3800 (2012)
56. Schwenck, N., Flemisch, B., Helmig, R., Wohlmuth, B.I.: Dimensionally reduced flow models in fractured porous media: crossings and boundaries. *Comput. Geosci.* **19**(6), 1219–1230 (2015)
57. Scott, L.R., Zhang, S.: Finite element interpolation of nonsmooth functions satisfying boundary conditions. *Math. Comput.* **54**(190), 483–493 (1990)
58. (SKI), S.N.P.I.: The international hydrocoin project - background and results. OECD. Paris, France (1987)
59. Tunc, X., Faille, I., Gallouët, T., Cacas, M.C., Havé, P.: A model for conductive faults with non-matching grids. *Comput. Geosci.* **16**(2), 277–296 (2011)